

Generative Adversarial Gumbel MCTS for Abstract Visual Composition Generation

Zirui Zhao^{1*} Boye Niu^{2*} David Hsu¹ Wee Sun Lee¹

¹National University of Singapore ²University of Sydney

ziruiz@u.nus.edu

Abstract

We study **abstract visual composition**, in which identity is primarily determined by the spatial configuration and relations among a small set of geometric primitives (e.g., parts, symmetry, topology). They are invariant primarily to texture and photorealistic detail. Composing such structures from **fixed components** under **geometric constraints** and **vague goal specification** (such as text) is non-trivial due to combinatorial placement choices, limited data, and discrete feasibility (overlap-free, allowable orientations), which create a sparse solution manifold ill-suited to purely statistical pixel-space generators. We propose a constraint-guided framework that combines explicit geometric reasoning with neural semantics. An AlphaGo-style search enforces feasibility, while a fine-tuned vision-language model scores semantic alignment as reward signals. Our algorithm uses a policy network as a heuristic in Monte-Carlo Tree Search and fine-tunes the network via search-generated plans. Inspired by the Generative Adversarial Network, we use the generated instances for adversarial reward refinement. Over time, the generation should approach the actual data more closely when the reward model cannot distinguish between generated instances and ground-truth. In the Tangram Assembly task, our approach yields higher validity and semantic fidelity than diffusion and auto-regressive baselines, especially as constraints tighten.

1. Introduction

Abstract visual concepts, those defined by structural relations among primitives rather than by rich texture or appearance, underlie many forms of human reasoning, communication and design. For example, architectural blueprints, engineering schematics, iconography and signage compose meaning from simplified geometric forms across contexts. We therefore foreground *visual composition*: meaning emerges from how simple parts are arranged into struc-

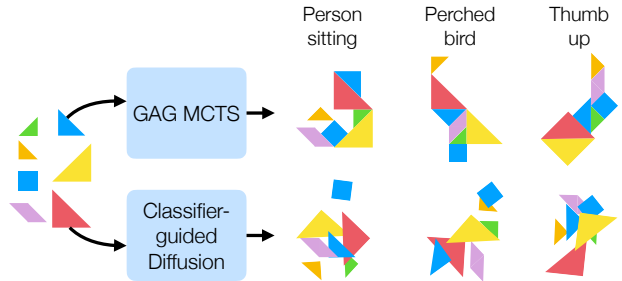


Figure 1. The Tangram assembly task. The seven pieces are placed on the board to form the target shape, described by the text prompt such as “perched bird”. We show that our GAG MCTS can generate semantically aligned abstract visual concepts under hard constraints and limited data, while diffusion models perform poorly.

ture. We call a visual concept *abstract* when its identity is specified primarily by structural regularities over simple primitives (shape, part relations, closure, symmetry), consistent with structural accounts and Gestalt principles of perceptual organisation [3, 50]. In this paper, we study composition explicitly by assembling fixed geometric pieces into target silhouettes or layouts from weak language cues (e.g., “bird,” “boat”), e.g., Tangram Assembly in Fig 1.

Composing with fixed pieces under geometric constraints differs fundamentally from naturalistic synthesis. First, feasibility is *discrete and brittle*: a single overlap or misalignment invalidates a composition; the feasible set is sparse and highly non-convex. Second, search is *combinatorial*: at each step, the system must choose which piece, where, and how to orient it while preserving future flexibility. Related packing/cutting problems are NP-hard even in simplified rectangular settings, underscoring intrinsic difficulty [16, 22]. Third, semantics are *underspecified*: textual prompts imply global shape regularities without prescribing unique layouts. Data-driven generators trained to match pixel statistics (e.g., diffusion, latent diffusion) excel at appearance but struggle to *guarantee* hard constraints or discover valid layouts from limited supervision [19, 42]. Object-centric auto-regressive transformer approaches ar-

*Equal contribution.

gue for compositional structure, but still lack exact constraint enforcement during synthesis [35].

To address these challenges, we propose an AlphaGo-like framework that integrates hard constraints into Monte Carlo Tree Search (MCTS) and employs a vision-language model to assess whether a generated configuration matches the textual goal. The key assumption is that validating an abstract visual composition is easier than learning to compose it directly. Prior work shows that fine-tuned vision-language models can reach human-level accuracy in recognising abstract tangram shapes [25], suggesting their suitability as reward models for evaluating candidate solutions.

Our method adopts an AlphaGo-style algorithm [47], where hard constraints are embedded in the transition model to prune infeasible actions. A fine-tuned CLIP model [40] serves as the reward function, measuring the semantic alignment between the final assembly and the goal description. Because such scorers may be permissive or inconsistent on out-of-distribution samples, we introduce adversarial reward refinement to better distinguish valid from near-miss compositions. The policy guiding MCTS is trained using Proximal Policy Optimisation [45] (PPO) with the refined reward, and the resulting policy is further used to generate hard negative examples for continued adversarial reward refinement. This framework enhances sample efficiency through constraint-based pruning and improves semantic faithfulness by leveraging language-aligned visual features.

We evaluate on **Tangram assembly**: seven fixed pieces must depict a textual concept; this probes joint semantic and geometric competence. We found that methods without search are limited in generating semantically aligned abstract visual concepts. To better understand the issues, we relax the problem into a **rectangle composition** task, where a composition is semantically valid if all pieces lie within a bounded area of width and height specified by the text. We found that the diffusion model and PPO achieved great performance in generation with weak geometrical constraints, but performed poorly with tight geometrical constraints. Across both, the proposed search-based generator achieves higher geometric validity and semantic agreement than diffusion and autoregressive baselines, with gains increasing under tighter constraints [22].

In summary, we proposed a hybrid method combining constraint-aware search with language-aligned visual rewards and adversarial refinement, specifically for abstract visual composition under hard constraints and limited data. Our method performs substantially better in Tangram assembly and rectangle composition problems than diffusion, auto-regressive transformer, and PPO-based methods.

2. Related work

Abstract visual reasoning. Abstract visual concepts are intangible ideas or notions that lack a physical form or concrete attributes. They cannot be directly perceived and typically denote qualities, relationships, or processes [4]. Those concepts have long been used to explore how people collaborate in communication when there are no established naming conventions, dating back to [30]. Tangrams were introduced as a research tool by [9]. Although these figures are composed of the same seven basic shapes, they inspire a diverse range of figurative descriptions, reflecting different ways of conceptualising them [2, 5, 13, 20, 21]. A recent study [25] focuses on the tangram reasoning for classification purposes using modern vision-language models. Those models process multimodal data through joint encoding, which captures richer interactions [7, 28, 36], or separate encoding, which is more flexible [26, 41].

For generating/visualising abstract visual concepts, there are a much smaller number of studies. Some research works use a diffusion model to generate images with abstract style or vector format (e.g., SVG) given language descriptions [15, 23, 43, 51, 53] or photo-realistic images [31, 37]. Some studies [10, 17, 32, 34, 48, 52] also focus on visualising highly abstract concepts with metaphor, which is highly subjective and does not focus on generating abstract representations of concrete objects. These works treat the language or image input as soft constraints, and many are very successful. However, neither of them had the hard geometrical constraints for their generation tasks.

Constrained Generation. Constrained generation is increasingly important for outputs that must satisfy geometric or physical rules. Methods incorporate constraints during training or inference, including geometric-loss GANs [57] and factor-graph layouts [14]. In CAD and mechanical design, models such as SketchGen [39] emit primitives plus constraints for downstream solvers; dual-discriminator GANs [1] and parameter-efficient models [38] target mechanical and geometric validity. Together, these works integrate domain constraints into generative pipelines, improving reliability.

Diffusion models show promise but struggle to enforce hard geometric rules: denoising approximates constraints without guarantees. Post-hoc projections (mirror mapping [33], optimisation-based sampling [8]) remain approximate and can fail under novel configurations; training-free fixes [56] add heuristics without verification. Without explicit geometric representations, constraints become negotiable preferences—unacceptable in precision domains (e.g., mechanical design). Recent MCTS-guided diffusion planning [55] uses rewards, but its action space still depends on diffusion via two meta actions (GUIDE/NO_GUIDE), keeping hard constraints implicit and unenforced.

3. Abstract Visual Composition

We formulate abstract visual composition under constraints using planning terminology. Let S be the state space representing all possible configurations of compositions (e.g., images, text, code) and A be the action space consisting of composition operations. Each state $s \in S$ must satisfy a set of hard constraints $C(s)$, which could include structural constraints (e.g., geometric constraints in tangram assembly), syntactic constraints (e.g., grammar rules in text generation), or logical constraints (e.g., type checking in code generation). Given a specification $y \in Y$, the constrained composition problem can be formulated as:

$$\text{find } s \in S \quad (1)$$

$$\text{s.t. } C(s) = \text{True} \quad (2)$$

$$G(s, y) = \text{True} \quad (3)$$

where $C(s)$ represents the domain-specific constraints that must be satisfied, and the goal function $G(s, y)$ determines whether state s fulfils the requirements specified by y . The transition function $T(s, a)$ captures how composition actions $a \in A$ transform the state s .

This formulation encompasses various constrained composition tasks. In tangram assembly, seven fixed pieces must be arranged to match a text-specified concept under geometric constraints: S is the space of layouts using two small triangles, one medium triangle, two large triangles, one square, and one parallelogram; Y is the space of natural-language descriptions of shapes; and the constraints $C(x)$ require (1) *each piece connects to at least one other*, (2) *no overlaps*, (3) *all seven pieces are used*. In constrained text generation, S could be sequences of tokens with syntactic or semantic constraints; in program synthesis, S might be programs that must satisfy both syntactic and semantic requirements.

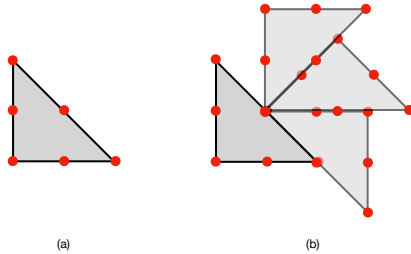


Figure 2. The demo of the actions in Tangram assembly. (a) The pieces can only be placed when their anchor points align; (b) rotations are restricted to multiples of 45 degrees.

For each assembly step, one piece can be placed adjacent to an already placed piece. To make the action space tractable, we discretise the possible placements: 1) *each piece has anchor points defined as its vertices and edge*

midpoints; 2) *pieces can only be placed when their anchor points align*; 3) *rotations are restricted to multiples of 45 degrees*. Example actions are demonstrated in Figure 2. Under these discretisation rules, the total valid action space contains approximately 3000 unique actions. The requirement function $R(x, y)$ evaluates whether the assembled configuration x matches the given text description y .

4. Generative Adversarial Gumbel MCTS

The core idea of our approach is based on the assumption that abstract visual composition is computationally hard to solve, but easy to verify if the solution is correct. We fine-tune the pre-trained vision language model as the reward model for verifying if the generated tangram configurations match the descriptions. The verification is computationally more efficient than finding such a tangram configuration.

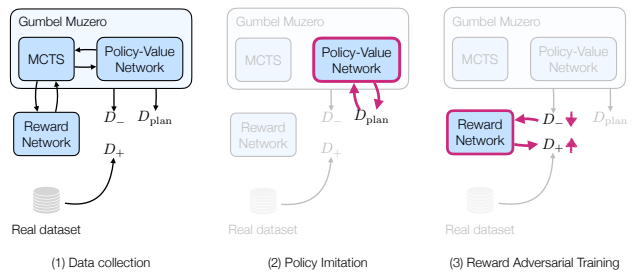


Figure 3. Demonstration of the proposed Generative Adversarial Gumbel MCTS. The black arrows indicate output data from the modules, and the purple arrows indicate gradient descent training.

As such, we leverage Monte-Carlo Tree Search to search and generate the configurations under geometrical constraints and use the reward model to provide reward signals that guide the MCTS process. The method is demonstrated in Figure 3. We use the MCTS in Gumbel MuZero, the latest variant of the AlphaZero algorithm, in our implementation. It learns a policy network as a search heuristic and a value network for the rollout of MCTS. We first fine-tune the reward network on the training dataset using contrastive learning. Then, during the Gumbel MuZero algorithm, we collect the preference dataset by using the generated configurations by MCTS as the negative instance D_- and the configurations in the training data as the positive instance D_+ . We then conduct adversarial training further to fine-tune the reward network for generative adversarial training, making it more robust and pushing the distribution of the generated configurations closer to that of the training dataset. See Appendix A for the details of Gumbel MuZero.

The actual implementation and network design are determined by the actual task setting and its characteristics. We introduce our network choices and loss function for our two experiments below.

4.1. Policy-value network

Inspired by the vision-language-action network (VLA) in robotics, we use a similar structure for our policy and value network. The overall structure of the network is shown in Fig 4.

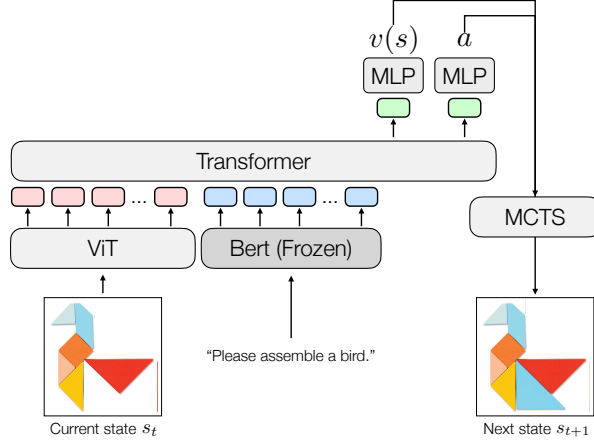


Figure 4. The policy value network. We use a pre-trained Vision Transformer (ViT) and Bert, together with a transformer that fuses the vision and language features, to form the main body of the network. We use a single network to predict the value and next action, as suggested by the AlphaZero paper. The last two tokens are decoded as a value and action logits after a linear layer.

In this network, we use a pre-trained Vision Transformer (ViT) and Bert, together with another transformer, to fuse the vision and language features and then decode the value prediction and action prediction. This network is used to imitate the planning trajectories generated from MCTS, and also learn the resulting value of the trajectories. After learning, the network can be used as a search heuristic and rollout function in MCTS for further improvement.

We design the structure of the network for a few reasons. First, our problem does not have a massive dataset, such as language modelling, for large-scale training. Thus, we do not need a large pre-trained transformer model such as Llama, and a model like Bert and regular-sized ViT would be enough. The structure is inspired by OpenVLA, which also utilises ViT as the image encoder and fine-tunes it during training. The difference is that we are not directly using the language model to fuse the text and image features, but we use a fixed Bert model to produce semantic features in text and fuse the embedding features of the text with the image features. The reason is still due to the limited data, and we wish to have a stable text feature representation that does not overfit the small training dataset. When combined with the search algorithm, the policy network acts as a search heuristic that prunes the Monte Carlo Tree Search, such as avoiding unlikely actions during the tree search and focus-

ing more on the more promising choices based on its previous search experience.

4.2. Reward network

We use the pre-trained vision language model, CLIP, as the reward network. The reward network takes the tangram configuration and text description as inputs and outputs a scalar value to evaluate the inputs' matching.

First, we use the training data in the Tangram dataset to fine-tune the pre-trained CLIP model using contrastive learning. It can achieve near-human accuracy when tested in the validation and testing datasets, as reported in the original paper. However, when we conducted the Gumbel Muzero training, we found that the generated tangram configurations can get a very high reward, but the shape of the tangram does not actually match the text description. Thus, the fine-tuned reward model is not very robust and can be easily fooled by false-positive instances.

To tackle the issue, we use generative adversarial training to push the reward model to give high rewards to instances that are similar enough to the distribution of the training dataset. We treat the generated tangram configuration as the negative instance and the labelled configuration as the positive instance, and conduct binary cross-entropy learning:

$$\begin{aligned} \mathcal{L}_{\text{pref}} = & -\frac{1}{N} \sum_{(\ell_i, s_i^+) \in D_+} \log(\text{sigmoid}(r_\phi(\ell_i, s_i^+))) \\ & -\frac{1}{N} \sum_{(\ell_i, s_i^-) \in D_-} \log(1 - \text{sigmoid}(r_\phi(\ell_i, s_i^-))) \end{aligned} \quad (4)$$

r_ϕ denotes the CLIP and ϕ denotes the parameter of the CLIP model. s_i denotes the tangram image and ℓ_i denotes the corresponding text description. The D_+ denotes the original dataset for image-text pairs, and D_- denotes the generated images given the text description. N is the batch size. To avoid catastrophic forgetting, we combine the loss with the contrastive loss of the training dataset.

$$\begin{aligned} \mathcal{L}_{\text{cont}} = & -\frac{1}{N} \sum_i \log \frac{\exp(v_i \cdot w_i / T)}{\sum_j \exp(v_i \cdot w_j / T)} \\ & -\frac{1}{N} \sum_j \log \frac{\exp(v_i \cdot w_j / T)}{\sum_i \exp(v_i \cdot w_i / T)} \end{aligned} \quad (5)$$

The contrastive loss samples image-text pairs from D_+ and extracts the image features v_i and text features w_i using CLIP. N is the batch size. Thus, the total loss for reward network training is controlled by $\mathcal{L}_{\text{pref}} + \lambda \mathcal{L}_{\text{cont}}$, where λ is a hyperparameter.

4.3. Gumbel MCTS with Adversarial Reward Refinement

We found that training a reward network with limited data is insufficient to produce stable and reliable reward signals; in many cases, the generated instances are invalid while the network still assigns high reward scores. To improve its reliability, we apply adversarial refinement that encourages the reward network to better discriminate between valid and near-miss samples, making its outputs more consistent with the training data distribution. With the refined reward network and the policy-value network, we perform the Generative Adversarial Training (Alg. 1). The framework iteratively generates planning trajectories and final tangram configurations using the current networks, then fine-tunes the policy-value network for improvement. We can use either PPO or MuZero as the improvement operator, though PPO tends to train faster in practice. The generated tangram configurations serve as negative instances for adversarial fine-tuning of the reward network, enabling mutual improvement between policy learning and reward refinement.

Algorithm 1 Generative Adversarial Training for Policy and Reward Network

- 1: **Require:** dataset for positive instances D_+ , policy-value network π_θ , reward network π_r
- 2: Fine-tune the reward model π_r using D_+ by optimising $\mathcal{L}_{\text{cont}}$
- 3: **while** not converge **do**
- 4: Randomly generate initial states from D_+
- 5: Use $\text{MCTS}(\pi_\theta)$ to generate negative instances D_- and planning trajectories D_{plan}
- 6: Use D_{plan} to finetune π_θ
- 7: Sample from D_+ and D_- to finetune r_ϕ by optimising $\mathcal{L}_{\text{pref}} + \lambda \mathcal{L}_{\text{cont}}$
- 8: **end while**
- 9: **return** π_θ and r_ϕ

Generative Adversarial training has difficulty converging as it is sensitive to hyperparameter choices. Thus, we choose to use a small gradient descent step for fine-tuning the reward model. This is also the reason why we chose the Gumbel MuZero, as it has better policy improvement in practice. Thus, we suggest using a relatively lower learning rate for reward fine-tuning and increasing the number of simulation steps for running MCTS.

5. Experiment: Tangram Assembly

This experiment aims to test the effectiveness of different methods in the constrained generation tasks that require the help of the foundation model. The task is to generate the configurations of tangram pieces, where the semantic con-

straints are encoded in the text description. The text description is a combination of the shape of the tangram pieces and the geometrical constraints. The goal is to generate the configurations of tangram pieces that are semantically accurate to the text description. This experiment aims to verify our hypothesis that the foundation model’s common-sense knowledge can help the search algorithm to generate the configurations of tangram pieces that are semantically accurate to the text description.

5.1. Experiment setup

Dataset. We use the KiloGram dataset for the experiment. The KiloGram dataset contains thousands of tangram pieces with tens of thousands of text annotations. The dataset is initially designed for abstract visual concept comprehension, i.e., tangram classification. In our study, we modify the dataset for constrained generation, which is empirically much harder than recognition/classification, even with discretisation in the action space. Some example images with annotations in the dataset are shown in Fig 5.

Baseline. We validate our assumption that for constrained generation, search coupled with a verifier (i.e., reward network) outperforms an auto-regressive policy. Additionally, we tested the impact of generative adversarial training. Thus, for the experiment, we compare the performance with baselines below:

- **Random.** This baseline randomly generates the configurations of tangram pieces.
- **Auto-regressive transformer.** This baseline is to use the auto-regressive transformer to generate the configurations of the tangram pieces. We use the same architecture as the Gumbel-MuZero, but we replace the MCTS with the auto-regressive transformer. We also applied the same action masks as the GAG MuZero during inference to avoid obvious overlapping issues. However, the action masks only mask out part of the invalid actions, as the validity of actions is determined dynamically by the real state. See the appendix for more details. As such, the mask cannot fully avoid the overlapping of pieces.
- **Classifier-Guided Diffusion model.** This baseline is to use the classifier-guided diffusion model [12] to generate the configurations of the tangram pieces. We use the same neural network architecture as our method, but we replace the MCTS with the diffusion model. To make the comparison fair, we also design a differentiable classifier that encodes the geometrical constraints to guide the diffusion model to generate the configurations of tangram pieces. For more details, please refer to the Appendix D. We provide the results with different classifier guidance scales β : stronger scales β mean greater classifier guidance.
- **PPO + Mask (+ Adv).** This baseline follows the reinforcement learning (RL) post-training recipe for LLM reasoning. It first SFTs a policy network and uses RL to

finetune the policy. We add the same action mask in the transition function as the MCTS for fair comparison. We also add adversarial reward refinement to ablate the effect of MCTS.

- **Gumbel Muzero without Generative Adversarial Training (w\o GA).** This baseline utilises the initial reward network. For the Rectangle Composition task, the reward network is trained purely by the training dataset. For the Tangram Assembly task, it is a pretrained CLIP model fine-tuned by the KiloGram dataset and employs standard Gumbel Muzero for training.
- **Gumble Muzero Generative Adversarial Training without Pretrained CLIP (GA w\o pretrain).** This baseline utilises Generative Adversarial Training for the Gumbel-Muzero, but the reward network is trained from scratch, rather than fine-tuned based on the pre-trained CLIP model.

Metric. For Tangram assembly, we use the original dataset’s data splits for training, validation, and testing, ensuring consistency in our experimental setup. To guarantee a fair comparison, we evaluate the performance using an equal number of samples from the testing set. Our primary focus is on measuring the likelihood, similarity, and diversity of the generated image. We use the Fréchet Inception Distance (FID score) to evaluate the likelihood. Additionally, we employ a precision-recall evaluation metric commonly used in image generation research to assess the diversity and similarity of generated images. The precision-recall metric evaluates generative model quality by measuring coverage of the real data manifold in feature space. Images are processed through an Inception network to extract feature representations $f_r \in \mathbb{R}^d$ for real samples and $f_g \in \mathbb{R}^d$ for generated samples. For each real sample i , a neighbourhood radius τ_i is computed as the distance to its k -th nearest neighbour among other real samples. Precision measures the fraction of generated samples that fall within at least one real sample’s neighborhood: Precision = $\frac{1}{M} \sum_{j=1}^M \mathbb{I} [\exists i : \text{dist}(f_g^j, f_r^i) \leq \tau_i]$. Recall measures the fraction of real samples covered by at least one generated sample: Recall = $\frac{1}{N} \sum_{i=1}^N \mathbb{I} [\exists j : \text{dist}(f_g^j, f_r^i) \leq \tau_i]$, where N and M are the number of real and generated samples respectively, and $\mathbb{I}[\cdot]$ is the indicator function. This approach ensures generated samples remain close to real data regions while providing comprehensive coverage of the target distribution. We also measure the percentage of valid states to determine how well the generated images satisfy the hard geometrical constraints, i.e., no pieces overlap. Consistent with common practices in generative AI research, we extract image features using a pre-trained InceptionV3 model to compute both the FID score and the precision-recall metric. For comparison purposes, we also evaluate the model using a CLIP model fine-tuned on the KiloGram dataset. Since InceptionV3 was pre-trained on

a realistic dataset, its feature extraction may not be as effective on images with a significantly different distribution found in the KiloGram dataset. Therefore, we present results from both evaluation methods.

Implementation details. We use Jax to create and vectorise the Tangram assembly task. The MCTS is adapted from the MCTX package, which uses JAX to conduct parallelised batch training. For more details, please refer to Appendix D.

5.2. Main Result

We report the experimental results for the Tangram assembly task in Table 1. For this task, we evaluate the FID scores to evaluate the likelihood of the generated images and also compare the reward gain of different versions of the policy. We also quantitatively evaluate the diversity of the generated images via the precision-recall metric in image generation evaluation. Furthermore, in our method (GA Gumbel Muzero), we also compared different versions with various levels of Gumbel noise. We summarise the experimental findings in the following paragraphs.

Table 1. Results on Tangram Assembly. t means the temperature of sampling, β is the classifier scale, and g means the Gumbel scale in Gumbel Muzero.

	FID \downarrow	FID $_{\text{clip}}\downarrow$	Pre \uparrow	Rec \uparrow	Val(%) \uparrow
Random	35.8	0.71	0.380	0.231	0.3
Auto-reg ($t = 1.0$)	28.6	0.59	0.580	0.410	54.2
Auto-reg ($t = 0.5$)	24.5	0.52	0.571	0.427	59.3
Auto-reg (Greedy)	23.2	0.48	0.564	0.424	61.1
Auto-reg+mask ($t = 1.0$)	25.0	0.57	0.553	0.409	87.9
Auto-reg+mask ($t = 0.5$)	23.1	0.50	0.575	0.430	88.1
Auto-reg+mask (Greedy)	22.0	0.48	0.568	0.423	86.4
PPO+mask (Greedy)	19.7	0.45	0.553	0.311	99.3
PPO+adv+mask (Greedy)	18.6	0.42	0.587	0.402	99.3
Diffusion ($\beta = 0.1$)	34.4	0.54	0.347	0.211	0.0
Diffusion ($\beta = 1.0$)	34.0	0.53	0.368	0.239	1.6
Diffusion ($\beta = 10.0$)	33.2	0.59	0.370	0.248	4.3
Gumbel Muzero w\o GA	22.9	0.46	0.569	0.412	98.5
GA w\o pretrain	32.3	0.53	0.503	0.491	98.5
GAG MCTS ($g = 1.0$)	18.2	0.41	0.576	0.459	99.3
GAG MCTS ($g = 0.5$)	17.6	0.40	0.585	0.451	98.5
GAG MCTS (Greedy)	16.8	0.39	0.591	0.444	99.3

Auto-regressive policies underperform; PPO improves validity but still underperforms search. In Tangram assembly, auto-regressive samples often overlap and do not match the text, with higher FID and lower precision/recall. Using the same partial action mask that filters roughly 80% of invalid actions, PPO post-training markedly increases non-overlap validity compared to the SFT auto-regressive policy (from $\approx 86\text{--}88\%$ to 99.3%) and matches the search baseline on validity (99.3%). Adversarial re-

ward refinement further improves precision modestly, but FID and precision/recall remain worse than search.

Diffusion performs badly with data scarcity. In our experiments, the diffusion baseline faces data scarcity issues, as there is only a limited training dataset for the text descriptions and final shapes. The diffusion tends to overfit the limited data, making it hard to generalise to novel descriptions. In addition, we found that even after massive training and strong gradient guidance, it still cannot satisfy the geometrical constraints. This might partially due to the small number of training data, but still shows the inherent limitation of diffusion model in constrained generation.

Search significantly helps the constrained generation. With the search algorithm, our method has a high FID score in tangram assembly, and the configuration has very low chances of violating the geometrical constraints.

The reward network is not robust without Generative Adversarial training. The Gumbel Muzero without Generative Adversarial Training has low reward gains and also relatively higher FID and lower precision and recall. All of the evidence suggests that the distribution of generated images is low in the labelled dataset.

The reward model suffers from overfitting without pretraining. In our Tangram assembly tasks, the Gumbel Muzero with Generative Adversarial Training, but without pre-trained CLIP, has a low FID score. Without the pre-training, the CLIP model exhibits significant overfitting issues. The CLIP can only correctly recognise about 30% of the tangram shapes in the validation and testing dataset. In addition, it has a significantly lower precision, meaning that the generated instances are also not generalisable to the unseen cases. The pre-trained CLIP model provides prior knowledge to the reward network, which is crucial for generalisation, especially in cases of data scarcity.

With adversarial training, the generated images have a statistically more similar distribution to the labelled dataset. After forcing the Generative Adversarial Training, in Tangram Assembly, our method suggests a higher likelihood of the generative dataset (higher precision and lower FID), and it is also relatively more diverse (higher recall) than the baseline. We also show some pictures generated by GAG Muzero in Fig 5.

Gumbel noise improves the diversity of the generation. Gumbel Muzero can control the scale of Gumbel Noise to control the randomness. We found that a reasonable level of randomness is helpful to get higher diversity (higher recall). However, the recall is still significantly lower than precision, meaning that we have the **mode collapse** issue, a common issue for Generative Adversarial Networks with a limited dataset.

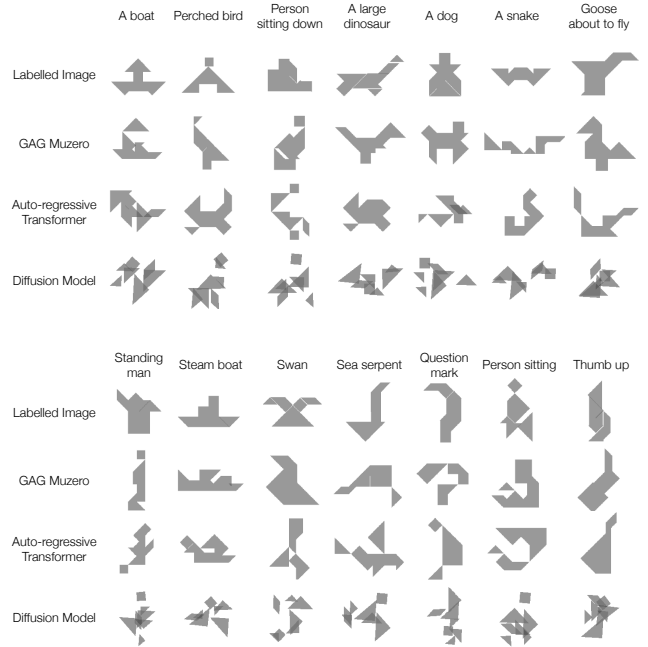


Figure 5. The demonstration of the dataset and the generated tangram configuration. We compare the configuration generated by GAG Muzero with the main baseline methods.

5.3. Human study

To evaluate the generation qualitatively, we conducted a small human study to know how good the generated Tangram configuration is when comparing with ground-truth configurations. We randomly sampled 50 pairs of generated and ground-truth tangram images with text description, and let 5 participants choose which one matches the text description better. For each pair of images, we show both of them on the screen and ask the participants: “Which image better matches the description below?” The results are shown in Table 2. Additional Details are in Appendix E.

Table 2. Result of human study. g is the Gumbel Scale, and t is the sampling temperature.

Preference v.s. GT (%)	
GAG Muzero ($g = 0.5$)	39.6 ± 3.9
Auto-Regressive ($t = 0.5$)	5.2 ± 2.7

Our small scale human study shows that participants choose substantially more Tangram shapes generated by GAG Muzero than the best baseline, showing that GAG Muzero generates reasonably well Tangram shapes to match the text description, even though it cannot make it perfect as some of the ground-truth images are really hard to beat.

6. Experiment: Rectangle Composition

In our Tangram experiments, it is difficult to disentangle the effects of hard constraints from goal ambiguity. We therefore study a relaxed abstract visual composition derived from Tangram: arrange a fixed set of rectangles within a text-specified rectangular region (abstract constraint learned from text) while satisfying a provided non-overlap constraint. Difficulty is controlled by the number/size of rectangles and the container dimensions. This experiment examines whether conclusions from Tangram persist here and how they vary with problem difficulty, and tests three hypotheses: (1) Generative models (auto-regressive transformers and diffusion models) handle weak or loosely defined constraints well but falter on complex geometric requirements; (2) search algorithms can explicitly encode hard geometric constraints in their action space; and (3) search-based methods will outperform generative approaches that must implicitly learn those constraints.

6.1. Experiment setup

Dataset. We generate synthetic rectangle packing problems using three piece types (1×2 , 2×3 , 1×5) with zero or 90-degree rotations. For each problem, we randomly sample target region dimensions (3×3 to 12×12) and use a randomised backtracking algorithm to find a complete tiling. We then randomly select 30-100% of the placed pieces to create packing problems of varying difficulty, ensuring each has at least one valid solution. The dataset contains 2,000 training, 100 validation, and 400 test configurations with different inventory distributions (training: five 1×2 , eleven 2×3 , two 1×5 pieces; validation/test: eight 2×1 , four 2×3 , six 1×5 pieces). Each configuration is centred at the origin and includes precise piece coordinates. We create easy and hard splits for the tasks. The easy tasks have fewer pieces to pack and the target region is larger, while the harder one has more pieces to pack in tighter spaces. We use the ratio of $r = \frac{\text{total area of pieces}}{\text{total area of target region}}$ to determine the difficulty: easy tasks have $r < 0.3$ while hard tasks have $r \geq 0.7$. For more details on data generation, please refer to Appendix C.

Metric. For rectangle composition, we mainly calculate the success rate of composition. A successful composition requires that the pieces have no overlap and that all the pieces are inside the target region.

6.2. Result

We report the results for the Rectangle composition in Table 3. We evaluate the success rate, where a successful instance should have all the pieces in the target region without overlapping, and the validity rate for the non-overlapping constraints. Overall, the conclusions largely mirror the Tangram Assembly results; the notable difference is that several methods perform reasonably well on easy rectangle tasks due to the relaxed setting.

Table 3. Results on Rectangle Packing (Success Rate % on the first three rows, valid rate % on the last row). t means the temperature of sampling, β is the classifier scale, and g means the Gumbel scale in Gumbel MCTS.

	Easy	Hard	Average	Valid
Auto-reg+Mask ($t = 1.0$)	55.50	2.00	28.75	84.25
Auto-reg+Mask ($t = 0.5$)	59.00	1.00	30.00	85.50
Auto-reg+Mask (Greedy)	51.50	1.50	26.50	88.50
PPO+Mask (Greedy)	89.50	13.00	51.25	94.50
PPO+Adv+Mask (Greedy)	94.00	30.00	62.00	95.50
Diffusion ($\beta = 0.1$)	89.00	21.50	55.25	70.50
Diffusion ($\beta = 1.0$)	93.50	19.50	56.50	75.50
Diffusion ($\beta = 10.0$)	97.00	15.50	56.25	82.75
GAG MCTS ($g = 1.0$)	95.50	50.50	73.00	98.50
GAG MCTS ($g = 0.5$)	95.00	53.50	74.25	97.75
GAG MCTS (Greedy)	96.00	51.00	73.50	95.25

Auto-regressive policies underperform on hard tasks; PPO helps but remains insufficient. Auto-regressive baselines are reasonably strong on easy cases but degrade sharply on hard ones, consistent with the findings of Tangram. PPO post-training increases validity on hard tasks, and adversarial refinement improves reward discrimination; yet, the policy still struggles to reliably satisfy goal constraints without search.

Diffusion is adequate on easy cases but fails under tight constraints. Diffusion performs well on easy rectangle compositions and generally stays within the target region, but breaks down when space is tight, even with strong guidance, which matches the Tangram conclusion, with only better performance on the easy split here.

Search substantially improves composition. Search achieves higher success rates by directly enforcing constraints and pruning invalid branches during planning, echoing the Tangram findings.

7. Conclusion

We focus on the abstract visual composition: composing fixed geometric pieces into target silhouettes or layouts from weak language cues. We show that combining constraint-aware search with a vision-language reward yields reliable compositions under strict geometric constraints. Our GAG MCTS employs a foundation model as a learned reward to guide MCTS: search enforces discrete feasibility, while the reward captures language-driven semantics. Across Tangram assembly and a relaxed rectangle-composition variant with adjustable difficulty, our method outperforms diffusion, PPO, and autoregressive baselines, with larger gains as constraints become tighter. Limitations include the overfitting of the reward model to the training data and a potential mode collapse issue, which is typical

in GAN-style methods, as well as the computational cost of search at high difficulty. Future work includes stronger verifiers (hybrid learned and formal checks), richer composition spaces (continuous placements and 3D CAD), and human-in-the-loop preference refinement to mitigate reward mis-specification.

References

- [1] Waad Almasri, Dimitri Bettebghor, Fakhreddine Ababsa, and Florence Danglade. Shape related constraints aware generation of mechanical designs through deep convolutional gan. *arXiv preprint arXiv:2010.11833*, 2020. [2](#)
- [2] Adrian Bangerter, Eric Mayor, and Dominique Knutson. Lexical entrainment without conceptual pacts? revisiting the matching task. *Journal of Memory and Language*, 114: 104129, 2020. [2](#)
- [3] Irving Biederman. Recognition-by-components: A theory of human image understanding. *Psychological Review*, 94(2): 115–147, 1987. [1](#)
- [4] Anna M Borghi, Samuel Shaki, and Martin H Fischer. Abstract concepts: External influences, internal constraints, and methodological issues. *Psychological Research*, 86(8): 2370–2388, 2022. [2](#)
- [5] Lucía Castillo, Kenny Smith, and Holly P Branigan. Interaction promotes the adaptation of referential conventions to the communicative context. *Cognitive science*, 43(8):e12780, 2019. [2](#)
- [6] Lili Chen, Kevin Lu, Aravind Rajeswaran, Kimin Lee, Aditya Grover, Misha Laskin, Pieter Abbeel, Aravind Srinivas, and Igor Mordatch. Decision transformer: Reinforcement learning via sequence modeling. *Advances in neural information processing systems*, 34:15084–15097, 2021. [13](#)
- [7] Zhenfang Chen, Peng Wang, Lin Ma, Kwan-Yee K Wong, and Qi Wu. Cops-ref: A new dataset and task on compositional referring expression comprehension. In *Proceedings of the IEEE/CVF Conference on Computer Vision and Pattern Recognition*, pages 10086–10095, 2020. [2](#)
- [8] Jacob K Christopher, Stephen Baek, and Nando Fioretto. Constrained synthesis with projected diffusion models. *Advances in Neural Information Processing Systems*, 37: 89307–89333, 2024. [2](#)
- [9] Herbert H Clark and Deanna Wilkes-Gibbs. Referring as a collaborative process. *Cognition*, 22(1):1–39, 1986. [2](#)
- [10] João M Cunha, Nuno Lourenço, Pedro Martins, and Peñousal Machado. Visual blending for concept representation: A case study on emoji generation. *New Generation Computing*, 38(4):739–771, 2020. [2](#)
- [11] Ivo Danihelka, Arthur Guez, Julian Schrittwieser, and David Silver. Policy improvement by planning with gumbel. In *International Conference on Learning Representations*, 2022. [12](#)
- [12] Prafulla Dhariwal and Alexander Nichol. Diffusion models beat gans on image synthesis. *Advances in neural information processing systems*, 34:8780–8794, 2021. [5](#)
- [13] Melissa C Duff, Julie Hengst, Daniel Tranel, and Neal J Cohen. Development of shared information in communication despite hippocampal amnesia. *Nature neuroscience*, 9(1): 140–146, 2006. [2](#)
- [14] Mohammed Haroon Dupty, Yanfei Dong, Sicong Leng, Guoji Fu, Yong Liang Goh, Wei Lu, and Wee Sun Lee. Constrained layout generation with factor graphs. In *Proceedings of the IEEE/CVF Conference on Computer Vision and Pattern Recognition*, pages 12851–12860, 2024. [2](#)
- [15] Kevin Frans, Lisa Soros, and Olaf Witkowski. Clipdraw: Exploring text-to-drawing synthesis through language-image encoders. *Advances in Neural Information Processing Systems*, 35:5207–5218, 2022. [2](#)
- [16] Michael R. Garey and David S. Johnson. *Computers and Intractability: A Guide to the Theory of NP-Completeness*. W. H. Freeman & Co., San Francisco, CA, 1979. [1](#)
- [17] Songwei Ge and Devi Parikh. Visual conceptual blending with large-scale language and vision models. *arXiv preprint arXiv:2106.14127*, 2021. [2](#)
- [18] Emil Julius Gumbel. Statistical theory of extreme value and some practical applications. *Nat. Bur. Standards Appl. Math. Ser. 33*, 1954. [12](#)
- [19] Jonathan Ho, Ajay Jain, and Pieter Abbeel. Denoising diffusion probabilistic models. In *Advances in Neural Information Processing Systems (NeurIPS 33)*, pages 6840–6851, 2020. [1](#)
- [20] Judith Holler and Katie Wilkin. Co-speech gesture mimicry in the process of collaborative referring during face-to-face dialogue. *Journal of nonverbal behavior*, 35:133–153, 2011. [2](#)
- [21] William S Horton and Richard J Gerrig. Speakers’ experiences and audience design: Knowing when and knowing how to adjust utterances to addressees. *Journal of Memory and Language*, 47(4):589–606, 2002. [2](#)
- [22] Manuel Iori, Vinícius L. de Lima, Silvano Martello, Flávio K. Miyazawa, and Michele Monaci. Exact solution techniques for two-dimensional cutting and packing. *European Journal of Operational Research*, 289(2):399–415, 2021. [1, 2](#)
- [23] Ajay Jain, Amber Xie, and Pieter Abbeel. Vectorfusion: Text-to-svg by abstracting pixel-based diffusion models. In *Proceedings of the IEEE/CVF Conference on Computer Vision and Pattern Recognition*, pages 1911–1920, 2023. [2](#)
- [24] Eric Jang, Shixiang Gu, and Ben Poole. Categorical reparameterization with gumbel-softmax. *arXiv preprint arXiv:1611.01144*, 2016. [12](#)
- [25] Anya Ji, Noriyuki Kojima, Noah Rush, Alane Suhr, Wai Keen Vong, Robert Hawkins, and Yoav Artzi. Abstract visual reasoning with tangram shapes. In *Proceedings of the 2022 Conference on Empirical Methods in Natural Language Processing*, pages 582–601, 2022. [2](#)
- [26] Chao Jia, Yinfei Yang, Ye Xia, Yi-Ting Chen, Zarana Parekh, Hieu Pham, Quoc Le, Yun-Hsuan Sung, Zhen Li, and Tom Duerig. Scaling up visual and vision-language representation learning with noisy text supervision. In *International conference on machine learning*, pages 4904–4916. PMLR, 2021. [2](#)
- [27] Zohar Karnin, Tomer Koren, and Oren Somekh. Almost optimal exploration in multi-armed bandits. In *International*

conference on machine learning, pages 1238–1246. PMLR, 2013. 12

[28] Wonjae Kim, Bokyung Son, and Ildoo Kim. Vilt: Vision-and-language transformer without convolution or region supervision. In *International conference on machine learning*, pages 5583–5594. PMLR, 2021. 2

[29] Wouter Kool, Herke Van Hoof, and Max Welling. Stochastic beams and where to find them: The gumbel-top-k trick for sampling sequences without replacement. In *International Conference on Machine Learning*, pages 3499–3508. PMLR, 2019. 12

[30] Robert M Krauss and Sidney Weinheimer. Changes in reference phrases as a function of frequency of usage in social interaction: A preliminary study. *Psychonomic Science*, 1: 113–114, 1964. 2

[31] Tzu-Mao Li, Michal Lukáč, Michaël Gharbi, and Jonathan Ragan-Kelley. Differentiable vector graphics rasterization for editing and learning. *ACM Transactions on Graphics (TOG)*, 39(6):1–15, 2020. 2

[32] Jiayi Liao, Xu Chen, Qiang Fu, Lun Du, Xiangnan He, Xiang Wang, Shi Han, and Dongmei Zhang. Text-to-image generation for abstract concepts. In *Proceedings of the AAAI Conference on Artificial Intelligence*, pages 3360–3368, 2024. 2

[33] Guan-Horng Liu, Tianrong Chen, Evangelos Theodorou, and Molei Tao. Mirror diffusion models for constrained and watermarked generation. In *Thirty-seventh Conference on Neural Information Processing Systems*, 2023. 2

[34] Vivian Liu, Han Qiao, and Lydia Chilton. Opal: Multimodal image generation for news illustration. In *Proceedings of the 35th Annual ACM Symposium on User Interface Software and Technology*, pages 1–17, 2022. 2

[35] Francesco Locatello, Dirk Weissenborn, Thomas Unterthiner, Aravindh Mahendran, Georg Heigold, Jakob Uszkoreit, Alexey Dosovitskiy, and Thomas Kipf. Object-centric learning with slot attention. In *Advances in Neural Information Processing Systems (NeurIPS 33)*, pages 11525–11538, 2020. 2

[36] Jiasen Lu, Dhruv Batra, Devi Parikh, and Stefan Lee. Vilbert: Pretraining task-agnostic visiolinguistic representations for vision-and-language tasks. *Advances in neural information processing systems*, 32, 2019. 2

[37] Xu Ma, Yugian Zhou, Xingqian Xu, Bin Sun, Valerii Filev, Nikita Orlov, Yun Fu, and Humphrey Shi. Towards layer-wise image vectorization. In *Proceedings of the IEEE/CVF Conference on Computer Vision and Pattern Recognition*, pages 16314–16323, 2022. 2

[38] Guglielmo Padula, Francesco Romor, Giovanni Stabile, and Gianluigi Rozza. Generative models for the deformation of industrial shapes with linear geometric constraints: Model order and parameter space reductions. *Computer Methods in Applied Mechanics and Engineering*, 423:116823, 2024. 2

[39] Wamiq Para, Shariq Bhat, Paul Guerrero, Tom Kelly, Niloy Mitra, Leonidas J Guibas, and Peter Wonka. Sketchgen: Generating constrained cad sketches. *Advances in Neural Information Processing Systems*, 34:5077–5088, 2021. 2

[40] Alec Radford, Jong Wook Kim, Chris Hallacy, Aditya Ramesh, Gabriel Goh, Sandhini Agarwal, Girish Sastry, Amanda Askell, Pamela Mishkin, Jack Clark, et al. Learning transferable visual models from natural language supervision. In *Proceedings of the 38th International Conference on Machine Learning (ICML) 2021*, pages 8748–8763, 2021. 2

[41] Alec Radford, Jong Wook Kim, Chris Hallacy, Aditya Ramesh, Gabriel Goh, Sandhini Agarwal, Girish Sastry, Amanda Askell, Pamela Mishkin, Jack Clark, et al. Learning transferable visual models from natural language supervision. In *International Conference on Machine Learning*, pages 8748–8763. PMLR, 2021. 2, 13

[42] Robin Rombach, Andreas Blattmann, Dominik Lorenz, Patrick Esser, and Björn Ommer. High-resolution image synthesis with latent diffusion models. In *Proceedings of the IEEE/CVF Conference on Computer Vision and Pattern Recognition (CVPR) 2022*, page †, 2022. † Fill in actual page numbers. 1

[43] Peter Schaldenbrand, Zhixuan Liu, and Jean Oh. Styleclip-draw: Coupling content and style in text-to-drawing translation. *arXiv preprint arXiv:2202.12362*, 2022. 2

[44] Julian Schrittwieser, Ioannis Antonoglou, Thomas Hubert, Karen Simonyan, Laurent Sifre, Simon Schmitt, Arthur Guez, Edward Lockhart, Demis Hassabis, Thore Graepel, et al. Mastering atari, go, chess and shogi by planning with a learned model. *Nature*, 588(7839):604–609, 2020. 13

[45] John Schulman, Filip Wolski, Prafulla Dhariwal, Alec Radford, and Oleg Klimov. Proximal policy optimization algorithms. *arXiv preprint arXiv:1707.06347*, 2017. 2

[46] David Silver, Julian Schrittwieser, Karen Simonyan, Ioannis Antonoglou, Aja Huang, Arthur Guez, Thomas Hubert, Lucas Baker, Matthew Lai, Adrian Bolton, et al. Mastering the game of go without human knowledge. *nature*, 550(7676): 354–359, 2017. 12

[47] David Silver, Thomas Hubert, Julian Schrittwieser, Ioannis Antonoglou, Matthew Lai, Arthur Guez, Marc Lanctot, Laurent Sifre, Dharshan Kumaran, Thore Graepel, Timothy Lillicrap, Karen Simonyan, and Demis Hassabis. A general reinforcement learning algorithm that masters chess, shogi, and go through self-play. *Science*, 362(6419):1140–1144, 2018. 2

[48] Zhida Sun, Zhenyao Zhang, Yue Zhang, Min Lu, Dani Lischinski, Daniel Cohen-Or, and Hui Huang. Creative blends of visual concepts. *arXiv preprint arXiv:2502.16062*, 2025. 2

[49] David Tolpin and Solomon Shimony. Mcts based on simple regret. In *Proceedings of the AAAI Conference on Artificial Intelligence*, pages 570–576, 2012. 12

[50] Max Wertheimer. Untersuchungen zur lehre von der gestalt. ii. *Psychologische Forschung*, 4:301–350, 1923. In German. 1

[51] Ronghuan Wu, Wanchao Su, Kede Ma, and Jing Liao. Iconshop: Text-guided vector icon synthesis with autoregressive transformers. *ACM Transactions on Graphics (TOG)*, 42(6): 1–14, 2023. 2

[52] Ping Xiao and Simo Matias Linkola. Vismantic: Meaning-making with images. In *International Conference on Computational Creativity*, pages 158–165. Brigham Young University, 2015. 2

[53] Ximing Xing, Chuang Wang, Haitao Zhou, Jing Zhang, Qian Yu, and Dong Xu. Diffsketcher: Text guided vector sketch synthesis through latent diffusion models. *Advances in Neural Information Processing Systems*, 36:15869–15889, 2023. 2

[54] John I Yellott Jr. The relationship between luce’s choice axiom, thurstone’s theory of comparative judgment, and the double exponential distribution. *Journal of Mathematical Psychology*, 15(2):109–144, 1977. 12

[55] Jaesik Yoon, Hyeonseo Cho, Doojin Baek, Yoshua Bengio, and Sungjin Ahn. Monte carlo tree diffusion for system 2 planning. *arXiv preprint arXiv:2502.07202*, 2025. 2

[56] Stefano Zampini, Jacob Christopher, Luca Oneto, Davide Anguita, and Ferdinando Fioretto. Training-free constrained generation with stable diffusion models. *arXiv preprint arXiv:2502.05625*, 2025. 2

[57] Yang Zeng, Jin-Long Wu, and Heng Xiao. Enforcing imprecise constraints on generative adversarial networks for emulating physical systems. *Communications in Computational Physics*, 30(3):635–665, 2021. 2

A. Preliminary: Gumbel Muzero

Gumbel Muzero [11] is a variant of the AlphaZero [46] algorithm with a major modification in the MCTS algorithm. Instead of using the upper confidence bound, Gumbel Muzero uses sequential halving, which minimises simple regrets, for the root action selection. As such, it is guaranteed to have policy improvement even with the minimal number of simulations in MCTS during the training.

Gumbel-Top-k trick. Gumbel Muzero uses the Gumbel-Max trick [18, 24, 29, 54] to sample n actions without replacement:

$$(g \in \mathbb{R}^k) \sim \text{Gumbel}(0) \quad (6)$$

$$A_1 = \arg \max_a (g(a) + \text{logits}(a)) \quad (7)$$

...

$$A_n = \arg \max_{a \notin \{A_1, \dots, A_{n-1}\}} (g(a) + \text{logits}(a)). \quad (8)$$

Here, we use $\text{argtop}(g + \text{logits}, n) = \{A_1, A_2, \dots, A_n\}$ for the Gumbel-Top-k samples.

Sequential Halving with Gumbel. Sequential Halving [27] is a bandit algorithm for simple regret minimisation. It aims at maximising the Q -value of the last or the finally selected action in simulations, which differs from the cumulative regrets that maximise the Q from all n simulations [49].

Algorithm 2 Sequential Halving with Gumbel

```

1: procedure SEQHALGUMBEL( $s, N, K, g, \pi_\theta, f, \sigma$ )  $\triangleright$   $s$ : current state;  $N$ : simulation budget;  $K$ : num of sampled moves;  $g$ : samples of Gumbel variable;  $\pi_\theta$ : policy network;  $f$ : simulation function, take the state, action, and simulation budget and output the average return;  $\sigma$ : monotonically increasing transformation.
2:    $\text{Seq} \leftarrow \text{argtop}(g + \pi_\theta, K)$ 
3:   while  $|\text{Seq}| > 1$  do
4:     for  $a \in \text{Seq}$  do
5:        $q(s, a) \leftarrow f(s, a, \lfloor \frac{N}{|\text{Seq}| \times \log_2(K)} \rfloor)$ 
6:     end for
7:      $\text{Seq} \leftarrow \text{set of } \lceil \frac{|\text{Seq}|}{2} \rceil \text{ actions in } \text{Seq} \text{ with the largest } (g(a) + \pi_\theta(s, a) + \sigma(q(s, a)))$ 
8:   end while
9:   return the remaining action in  $\text{Seq}$ 
10: end procedure

```

The algorithm of Sequential Halving with Gumbel is shown in the Alg 2. The original Sequential Halving samples possible moves/actions from action space uniformly at random, while the author modified it to sample from a

learned policy network π_θ without replacement. The policy network π_θ can be viewed as a parameterized distribution over the action space, and θ is its parameter. It then simulates those sampled actions for $\lfloor \frac{N}{|\text{Seq}| \times \log_2(K)} \rfloor$ number of times each, selecting half of the actions with the highest average return, and repeats the process, until there is only one action remains.

Gumbel Muzero MCTS Using the Sequential Halving with Gumbel algorithm, the authors modified the action selection procedure in Monte Carlo Tree Search. The pseudocode is shown in Alg 3.

Algorithm 3 MCTS in Gumbel Muzero

```

1: procedure SEARCH( $s, N, k, g, \pi_\theta, \sigma, \tau$ )  $\triangleright$   $s$ : node for the current state;  $\tau$ : tree;  $N$ : num of simulation.
2:    $f \leftarrow \text{SIMULATE}(s, a, \tau, \text{False}, \text{depth}=0)$ 
3:   return SEQHALGUMBEL( $s, N, K, g, \pi_\theta, f, \sigma$ )
4: end procedure
5: procedure SIMULATE( $s, a, \tau, \text{done}, \text{depth}$ )
6:   if  $\gamma^{\text{depth}} < \epsilon$  or  $\text{done} = \text{True}$  then
7:     return 0
8:   end if
9:   if  $s$  is a leaf node then
10:    Update  $\tau$  by adding the new state node
11:     $\forall a \in A, N(s, a) \leftarrow 0, q(s, a) \leftarrow 0$ 
12:    return  $v_\theta(s)$ 
13:   end if
14:    $\pi' \leftarrow \text{softmax}(\pi_\theta + \sigma(q))$ 
15:    $a^* \leftarrow \arg \max_{a \in A} (\pi'(a) - \frac{N(a)}{1 + \sum_b N(b)}) \triangleright$  Action selection at non-root nodes
16:   Simulate action  $a^*$  from node  $s$  to get next state node  $s'$ , reward  $r$ , and  $\text{done}$ .
17:    $R \leftarrow r + \gamma \cdot \text{SIMULATE}(s', a^*, \tau, \text{done}, \text{depth} + 1)$ 
18:    $N(s, a^*) \leftarrow N(s, a^*) + 1, N(s) \leftarrow N(s) + 1$ 
19:    $q(s, a^*) \leftarrow q(s, a^*) + \frac{R - q(s, a^*)}{N(s, a^*)}$ 
20:   return  $R$ 
21: end procedure

```

Gumbel Muzero uses the new MCTS algorithm to perform the self-play with a policy network and value network and uses the generated planning data to train the policy network and value network for improvement. This variant of the MCTS algorithm has a better guarantee that the policy produced by MCTS is better than the policy network, i.e.,

$$q(s, \arg \max_{a \in \text{argtop}(g, \pi, k)} (g(a) + \pi(s, a) + \sigma(\bar{q}(s, a))) \geq q(s, \arg \max_{a \in \text{argtop}(g, \pi, k)} (g(a) + \pi(s, a))). \quad (9)$$

Where the \bar{q} is estimated by the MCTS algorithm and σ is a

transform function, such as the formula we used below:

$$\sigma(q(a)) = (c_{\text{visit}} + \max_b N(b))c_{\text{scale}}q(a). \quad (10)$$

The equation is equivalent to $\mathbb{E}_{a \sim \text{MCTS}}[q(s, a)] \geq \mathbb{E}_{a \sim \pi}[q(s, a)]$ according to the Gumbel-Max trick. Thus, Gumbel MuZero can improve the policy with even a minimal number of simulations in MCTS.

B. Action masks for Tangram assembly

The system employs a two-stage approach for handling valid actions in tangram puzzle solving. In the precomputation stage, valid actions are exhaustively generated by iterating through all possible piece combinations, transformations, and anchor point alignments. For each pair of pieces (moved and reference), the algorithm considers eight rotation states (0 to 315 degrees in 45-degree increments), up to 2 flip states (depending on piece symmetry), and anchor points derived from vertices and edge midpoints. The system validates each potential action by checking for geometric overlaps using polygon intersection tests. It removes duplicate actions based on relative configuration hashing that encodes piece positions, transformations, and anchor alignments. The resulting precomputed valid action list is stored as a JSON file and loaded at runtime.

During gameplay, action masks are dynamically computed, which apply contextual validity checks to the precomputed action list. These checks ensure that: (1) the moved piece is unplaced (all pose values are zero) while the reference piece is placed (at least one pose value is non-zero), (2) flip and rotation IDs are within valid ranges for each piece type, (3) anchor point indices are appropriate for the piece geometry (6 anchors for triangles, 8 for quadrilaterals), and (4) the reference piece’s flip state matches the current environment state. This hybrid approach balances computational efficiency by precomputing geometric constraints while maintaining runtime flexibility for state-dependent action filtering.

In order to apply the geometrical constraints, when overlaps happen, there will be a negative penalty to the search algorithm, such that it knows to avoid overlaps naturally.

C. Rectangle Packing Dataset Generation

Piece Definitions Three types of rectangular pieces are used: 1x2, 2x3, and 1x5, each with allowed 0° and 90° rotations. The pieces are defined by their grid cell coverage.

Inventory and Region Sampling For each dataset split (train, validation, test), a fixed inventory of pieces is specified. The target region is a rectangle with width and height sampled uniformly from a specified range, subject to the constraints that the area is even and does not exceed the total available piece area.

Tiling and Packing Generation A recursive backtracking search is used to find a complete tiling of the target region using the available inventory. To create a packing problem, a random subset of the pieces from the full tiling is selected, with the fraction to keep sampled uniformly from [0.3, 1.0].

Configuration Construction For each configuration, the target region dimensions, the set of pieces to pack, and the solution placements (including piece type, rotation, anchor position, and computed vertices) are recorded. All piece placements are centred by applying a global offset so that the region is centred at (0, 0).

Uniqueness and Output Each configuration is assigned a unique signature based on the region and piece set to ensure dataset diversity. Configurations are saved in JSON format for training, validation, and test splits. Example images are also generated for visualisation.

D. Implementation details

D.1. GAG MuZero

Framework: The Tangram Assembly GAG MuZero agent is implemented in JAX/Flax, leveraging distributed training across multiple devices. The environment simulates the sequential assembly of tangram pieces, with each state represented as an image and associated instruction tokens.

Model Architecture:

- **Policy/Value Network:** A Decision Transformer [6] backbone is used, with BERT-based text encoding and a vision transformer (ViT) for image processing. The network outputs action logits and value estimates.
- **Reward Model:** A CLIP-based [41] reward model computes the alignment between the assembled image and the instruction, using contrastive and pairwise preference losses.

Self-Play and Search:

- **Self-Play:** The agent generates training data via self-play, using a Gumbel MuZero Monte Carlo Tree Search (MCTS) [44] for action selection. The search incorporates a recurrent function that simulates environment transitions and model predictions.
- **Batching:** Self-play and training are parallelised across devices, with large batch sizes (e.g., 2048 for self-play).

Training:

- **Policy/Value Training:** The policy and value networks are trained using cross-entropy and mean squared error

losses, respectively, with targets computed from self-play trajectories.

- *Reward Model Training*: The reward model is updated using both contrastive and pairwise preference losses, encouraging correct alignment between images and instructions.
- *Optimisation* : Adam optimisers are used for both networks, with learning rates 5×10^{-5} (policy/value) and 1×10^{-8} (reward).
- *Checkpointing*: Models and optimizers are periodically checkpointed for recovery and evaluation.

D.2. Diffusion model: Rectangle Packing

Architecture: We employ a Transformer-based diffusion model for rectangle assembly. Each rectangle is represented by its state (x, y, θ) and shape (w, h) , with a global target shape as an additional condition. States and shapes are embedded via linear layers and combined, while the target shape is provided to the Transformer decoder as a separate memory token. The model predicts denoising updates for all rectangles in parallel.

Classifier Guidance: The sampling process incorporates differentiable guidance losses:

- *Angle Loss*: Encourages θ to be close to multiples of 90° .
- *Overlap Loss*: Penalises overlapping rectangles using a softplus function on pairwise distances.
- *Region Loss*: Penalises rectangles placed outside a specified bounding region.

Sampling: Diffusion sampling iteratively updates rectangle states using the model’s prediction and the gradient of the guidance loss. Typical parameters include 100 steps, a step size of 0.05, and a guidance scale of 1.0.

D.3. Diffusion model: Tangram Assembly

Architecture: For tangram assembly, we utilise a Transformer encoder-based diffusion model. Each piece is represented by $(x, y, \text{rotation}, \text{flip}, \text{index})$. CLIP text embeddings of the target description are projected and concatenated with piece embeddings before being processed by the Transformer. The model predicts noise for $(x, y, \text{rotation})$ only; flip and index are fixed.

Dataset: The dataset consists of tangram configurations paired with natural language descriptions. Each sample includes piece positions, types, and a binary target mask.

Guidance: The guidance loss combines:

- *Overlap Loss*: Penalises overlapping polygons using signed distance functions.
- *Angle Loss*: Encourages rotations to be multiples of 45° .

Diffusion Process: We use a Denoising Diffusion Probabilistic Model (DDPM) scheduler with 1000 timesteps. During training, the model is optimised to predict the added noise. During sampling, classifier guidance is optionally applied by backpropagating the guidance loss.

Training Details: Optimisation is performed using AdamW with a learning rate of 1×10^{-4} and cosine annealing. The batch size is 512. Validation is conducted periodically with visualisation and checkpointing.

D.4. Classifier Guidance Function

The classifier guidance function is designed to provide smooth, differentiable constraints during diffusion-based shape assembly. It combines multiple loss terms, such as angle alignment, overlap penalty, and region constraints, into a single scalar objective. The general form is:

$$f_{\text{guidance}}(\mathbf{s}, \mathbf{p}, \mathcal{R}) = \lambda_{\text{angle}} \mathcal{L}_{\text{angle}}(\theta) \quad (11)$$

$$+ \lambda_{\text{overlap}} \mathcal{L}_{\text{overlap}}(\mathbf{s}, \mathbf{p}) \quad (12)$$

$$+ \lambda_{\text{region}} \mathcal{L}_{\text{region}}(\mathbf{s}, \mathcal{R}) \quad (13)$$

where $f_{\text{guidance}}(\mathbf{s}, \mathbf{p}, \mathcal{R}) \approx 0$ for valid configurations and increases as constraints are violated. This function is used for gradient-based guidance during diffusion, rather than as a binary classifier. The \mathbf{s} are the current states (e.g., positions and angles of pieces), \mathbf{p} are the piece shapes, \mathcal{R} is the target region, λ_{angle} , λ_{overlap} , λ_{region} are weighting coefficients.

Angle Loss (Soft-Min to Target Angles)

$$\mathcal{L}_{\text{angle}}(\theta) = \sum_{i=1}^N \left(-\frac{1}{\beta} \log \sum_k \exp [-\beta(\theta_i - \theta_k^*)^2] \right) \quad (14)$$

where θ_k are the target angles (e.g., $0^\circ, 90^\circ, \dots$), and β controls the sharpness.

Overlap Loss (Softplus Penalty)

$$\mathcal{L}_{\text{overlap}}(\mathbf{s}, \mathbf{p}) = \frac{1}{2} \sum_{i \neq j} \text{softplus}(r_i + r_j - d_{ij}) \quad (15)$$

where d_{ij} is the distance between centers, r_i is the effective radius of piece i .

Region Loss (Softplus Boundary):

$$\begin{aligned} & \mathcal{L}_{\text{region}}(\mathbf{s}, \mathcal{R}) \\ &= \sum_{i=1}^N [\text{softplus}(x_{\min} - x_i) + \text{softplus}(x_i - x_{\max}) \\ & \quad + \text{softplus}(y_{\min} - y_i) + \text{softplus}(y_i - y_{\max})] \end{aligned} \quad (16)$$

where (x_i, y_i) is the position of piece i , and $(x_{\min}, x_{\max}, y_{\min}, y_{\max})$ define the region.

Table 4. The detailed human study results (per-participant choice counts). The numbers are the choice counts for the generated image and the ground-truth image.

	Participant 1	Participant 2	Participant 3	Participant 4	Participant 5
GAG Muzero (chosen)	19.0	21.0	16.0	21.0	21.0
Auto-Regressive (chosen)	3.0	1.0	4.0	1.0	2.0

E. Human Study Details

Our human study is conducted with 5 participants. We randomly sampled 50 pairs of generated and ground-truth tangram images with text description, and let 5 participants choose which one matches the text description better. For each pair of images, we show both of them on the screen and ask the participants: “Which image better matches the description below?”

One example question of the questionnaire is shown in Fig 6.

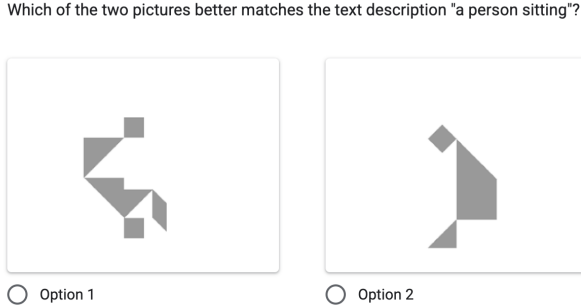


Figure 6. One example question in the questionnaire. We randomly sampled 50 pairs of generated and ground-truth tangram images with text description, and let 5 participants choose which one matches the text description better. For each pair of images, we show both of them on the screen and ask the participants: “Which image better matches the description below?” The placement of the image are random, i.e., the generated image can be placed on the left side or the right side.

The detailed result are shown in Table 4, including the choice counts for the generated image and the ground-truth image. For each participant, we randomly shuffle the pairs of images and let them choose the better one. The results are shown in the table.